Model for spin coating in microelectronic applications

R. K. Yonkoski and D. S. Soane

Citation: Journal of Applied Physics **72**, 725 (1992); doi: 10.1063/1.351859
View online: http://dx.doi.org/10.1063/1.351859
View Table of Contents: http://scitation.aip.org/content/aip/journal/jap/72/2?ver=pdfcov
Published by the AIP Publishing

Model for spin coating in microelectronic applications

R. K. Yonkoski and D. S. Soane
Department of Chemical Engineering, University of California, Berkeley, Berkeley, California 94720

(Received 14 January 1992; accepted for publication 6 April 1992)

A thorough investigation of the mass and momentum equations pertaining to the spin-coating process has been performed. A scaling analysis forms the foundation to determine the relevant characteristic quantities of the process and allows the assumptions and simplifications made by previous authors to be critically examined. Based on this analysis, the complete equations are reduced to a two-dimensional set of equations while retaining the essential physics of the problem. By further assuming a uniform film thickness over the disk, a one-dimensional model has been developed to assess the importance of the coupling between fluid flow and mass transfer during spin coating. The model predictions for the final film thickness can be presented in such a manner that the results superimpose onto one curve. In this way the film thickness and its relationships with process and material properties, initial solvent content, and spinning conditions can be succinctly expressed in terms of two characteristic parameters. The literature confusion over the exponent of the power-law dependence of the final film thickness on the rotational speed is also clarified. The model predicts an exponent of $-\frac{1}{2}$ which agrees with most experimental investigations. However, when the total spin time is too short, the exponent may deviate from $-\frac{1}{2}$. Finally, a split mechanism model that assumes that the spin-coating process could be divided into two stages, one where fluid flow is occurring exclusively and the other where only mass transfer occurs, has been shown to be quantitatively inaccurate.

I. INTRODUCTION

Spin coating of resist and polyimide films onto silicon wafers is an important step in the fabrication of integrated circuits. These films may be used for planarization and photolithography (sacrificial layers), or as interlayer dielectric insulators (permanent layers). A complete review of the process may be found elsewhere,[1] and we will include only a cursory review that emphasizes the points important for our discussion. The spin-coating process is carried out by dispensing a sufficient amount of liquid onto a wafer to flood it with the casting solution and then rapidly accelerating the wafer to the final spin speed. Rotation proceeds for a specified amount of time during which the film thins by a combination of fluid flow and evaporation. Finally, the disk is decelerated to rest. This procedure may then be followed by a baking step to remove residual solvent, or in the case of polyimide films, to cure the polymeric precursor to its desired final form.

Because of the importance and complexity of the spin-coating process, a considerable amount of effort has been directed to establish empirical relationships that describe the dependence of spin coating on process parameters. The basic result of these investigations was that the final film thickness h_f was proportional to a function of the initial solvent concentration C_0 and to some power of the rotational speed ω,[2–7]

$$h_f \sim f(C_0)\omega^b. \tag{1}$$

Often b was found to be $-\frac{1}{2}$, although some authors suggested that it depended on the evaporation conditions or viscosity ranges. Daughton and Givens[5,6] described an extensive experimental investigation of spin-coating parameters. They determined the film thickness to be independent of the amount of fluid dispensed, the disk rotational speed at which the fluid was dispensed, and the acceleration rate to the final spin speed. The film thickness, however, was found to depend strongly on the final rotational speed and initial solvent content as well as the material properties of the fluid.

Many attempts have been made at modeling the spin-coating process in varying degrees of complexity. The essence of these models[8–14] was to derive a kinematic expression for the film thickness,

$$\frac{\partial h}{\partial t} = -\frac{\rho\omega^2}{3\eta r}\frac{\partial(r^2h^3)}{\partial r} - \hat{e}. \tag{2}$$

Here h is the time-dependent film thickness, ρ is the solution density, η is the solution viscosity, r is the radial position, t is time, and $\hat{e}$ stands for film thinning due to solvent evaporation. The pioneering effort by Emslie and coworkers[8] described the film thinning behavior for a fluid where solvent evaporation did not occur. They found that a uniform film would remain uniform and that initially nonuniform film profiles would reduce to uniform films as spinning proceeded. The common result from models that included solvent evaporation was that the rate of film thinning is initially dominated by fluid convection and then by mass transfer.[12–16] This prompted many authors to claim that the spin-coating process can be effectively approximated by splitting it up into two time domains. During the first stage only fluid flow is allowed to occur, while in the second stage mass transfer occurs exclusively. We will show that significant errors can develop following this "split model" approach.

 0021-8979/92/140725-16$04.00

II. EXPERIMENTAL PROCEDURES

Spin-coating experiments were performed with two Du Pont polyimide precursor solutions, PI2525 and PI2545. Prior to spinning, the solutions were removed from a freezer and allowed to equilibrate thoroughly to room temperature. Dilutions were made using pure N-methyl-2-pyrrolidinone (NMP) solvent from Aldrich. Care was taken to minimize the exposure of the solvent and solutions to the atmosphere since NMP is extremely hygroscopic. The stock bottle of solvent was stored under nitrogen and small quantities were removed when required in a nitrogen glovebox.

The polymer films were made by spin coating the polyimide precursor film using a model P6024 tabletop precision spin coater by Integrated Technologies. The rotational speed ranged from 3000 to 8000 rpm and the acceleration and deceleration rates were set to their maximum values. The experiments were performed in a hood with the spin-coater lid off so that no accumulation of solvent vapor above the film would occur. A combination of 25 cm glass cover slips, 2 in. silicon wafers, and 4 in. silicon wafers was used as substrates. The glass cover slips were used when only qualitative trends were desired.

After spinning, most films were dried under vacuum in order to remove any remaining solvent until their weight no longer changed. The cured films were processed following the suggested schedule by the manufactures, namely a soft bake at 170 °C followed by a ramp to and cure bake at 400 °C. All weight measurements were made using a model GA110 Ohaus digital balance accurate to 0.1 mg. Approximate film thicknesses were calculated based on the weight, disk cross-sectional area, and initial density of the polyimide precursor solution. Also, film thickness measurements were performed at specific locations on the silicon wafers using an Tencor Alphastep 200 profilometer.

III. SPIN-COAT MODELING

The spin-coating process can be divided into three stages: deposition and spin up, spin off, and film drying. Although these stages overlap slightly, their physics can be effectively modeled by separating them into three distinct stages and treating their mathematics individually. This approach differs from the "split model" in that mass fluid flow and solvent evaporation are not restricted from occurring simultaneously.

A. Deposition and spin up

The liquid solution may be deposited in several different manners ranging from pouring the entire solution at the center of the disk and allowing it to spread radially over the film, to delivering the liquid in a steady stream moving radially over the rotating disk so that the deposited liquid forms a spiral. In all cases the amount of fluid deposited is such that the disk receives a large excess of fluid and is completely covered. Next, the disk is accelerated to its final rotational speed. It is here where the liquid undergoes a great deal of change from its initial state as a thick film essentially at rest to a thin film rotating with the disk.

TABLE I. Typical conditions on which the spin-coating model is based.

Parameter	Conditions
Rotational speed	2000–8000 rpm
Acceleration rate	impulse (as close as possible)
Dispense volume	large excess
Dispense manner	flood the entire disk with fluid
Viscosity range	initially 1–100 P

The majority of the liquid is sloughed from the disk as the disk is accelerated due to the overwhelming force of the centrifugal acceleration. Conversion to a thin, nearly uniform film takes place within the first second or two of spinning.

We also utilize the previously mentioned experimental results where the final film thickness has been shown experimentally to be independent of the manner of deposition, the amount of fluid dispensed, and the acceleration rate of the disk to its final spin speed.[5,6] However, if the disk is accelerated extremely slowly or if an insufficient amount of fluid is dispensed to cover the disk, then the final film thickness may indeed depend on these conditions.[14] Therefore, the deposition stage is assumed to take place under conditions typical of the microelectronic industry, specifically those indicated in Table I.

Operating within these experimental specifications, one can safely assume that the final film thickness will be independent of both the initial film profile and thickness, provided they are not too nonuniform or thin, respectively. This point has been confirmed by numerous theoretical models from the most simple[8,12,17,18] to the more complex.[9,11,13,14] Since these models differ in both assumptions and complexities, yet they all agree on this point, it must be taken to be an inherent fact in the physics and not just a byproduct of modeling assumptions. Also, the azimuthal velocity of the liquid film has been found to match almost instantaneously that of the rotating solid.[19] Finally, because of the limited time for evaporation, the solvent concentration has not deviated significantly from its original value. Therefore, we can assume that this stage of the spin-coating process merely sets up the next stage and the details of the mathematics are unimportant. What is important is that we are left with a reasonably uniform thin film rotating at the speed of the disk and with a solvent concentration essentially at its original value.

B. Spin off

During this stage the film is thinned due to a combination of convection and solvent evaporation. The centrifugal forces act to drive the fluid radially off the edge of the disk impeded only by the viscous resistance. This radial flow quickly diminishes because the film has become exceedingly thin and evaporation of solvent has increased the viscosity by several orders of magnitude. During fluid flow the film is also thinned by solvent evaporation to the overlying atmosphere. It is the trade-off between these two mechanisms that controls the film thickness, uniformity, and the success of the spin-coating process.

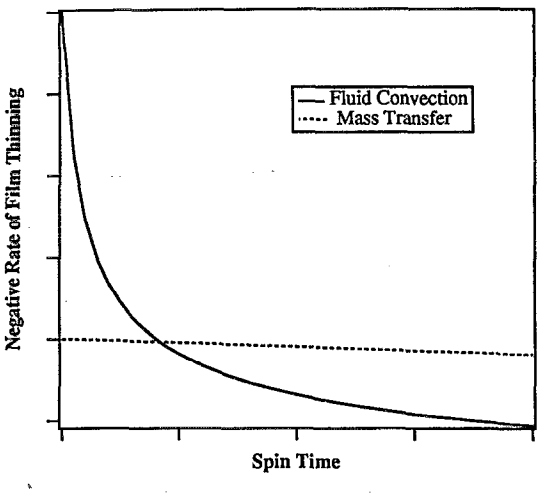

FIG. 1. Comparison of the different mechanisms for the rate of film thinning in arbitrary units. The fluid convection thinning arises from the force of the centrifugal acceleration, while the mass transfer loss results from solvent evaporation at the free surface.

It would be tempting at first to separate the spin-coating process into two separate mechanisms where there would be a sudden transition from pure centrifugally driven fluid flow to pure solvent evaporation. This idea has been used by several authors[10,12,18,20–24] and suggested by most others. The basis for this separation is that the rate of film thinning is dominated first by the centrifugal force and then by the solvent evaporation.[1,12,13] Figure 1 illustrates the typical competition between these mechanisms. The solvent evaporation, however, plays an important role during the flow-dominated regime through the strong concentration dependence of the viscosity. In fact, Jenekhe[15] concluded that the predominant effect of solvent evaporation is through the changing rheological properties of the system. Therefore, because the viscosity strongly depends on the solvent concentration profile, solvent evaporation can play a crucial role during the fluid flow regime and cannot *a priori* be separated from the spin-off stage.

C. Film drying

In this final stage of spin coating, fluid flow has essentially halted and further shrinkage of the film arises from solvent loss alone. Previously, the solvent concentration profiles depended on fluid convection flow through the cross terms in the solvent conservation equation. However, as the velocity components drop to zero, this dependence becomes unimportant, and solvent conservation may be considered independently. It is at this point where the spin-off stage ends and the film drying stage begins. We may continue to track the solvent concentration via the conservation equation or simply flash off any remaining solvent leaving a dry film behind. The former technique would be required when the film or underlying topography is not uniform because solvent diffusion may tend to modify existing free surface profiles.

D. Model development

The physics of the spin-coating process can be described by the incompressible equations of mass and momentum conservation and are enumerated below in their compact form:

$$\nabla\cdot\mathbf{v}=0, \tag{3}$$

$$\rho\frac{D\mathbf{v}}{Dt}=-\nabla p+\rho\mathbf{g}-\nabla\cdot\tau, \tag{4}$$

$$\frac{Dw_s}{Dt}=\nabla\cdot(D\nabla w_s), \tag{5}$$

where $\mathbf{v}$ is the fluid's velocity vector, p is the system pressure, $\mathbf{g}$ is the gravitational force vector, τ is the deviatoric stress tensor, and w_s is the weight fraction solvent. These equations are called the continuity, Cauchy momentum balance, and convective diffusion equations, respectively. One further equation is required for closure of the problem, namely a constitutive relationship relating the stress values to the relevant shear rates. A generalized Newtonian form,

$$\tau=-\eta(\nabla\mathbf{v}+\nabla\mathbf{v}^T), \tag{6}$$

can be chosen as it allows for shear thinning through a simple shear-dependent viscosity coefficient η. For a Newtonian fluid, η is independent of shear rate. Many polymeric solutions, however, exhibit shear thinning behavior that can be described by a phenomenological relationship between the viscosity coefficient and the shear rate of the fluid. One often quoted expression is the Carreau model,

$$\eta=\eta_f(1+\lambda^2 I_2)^{(n-1)/2}, \tag{7}$$

where η_f and λ are constants that depend only on the solvent weight fraction. I_2 is the second invariant of the deformation tensor, a measure of the shear rate.

In order to reduce this set of vector equations to a tractable set of differential equations, a number of simplifications and assumptions are employed: (i) The disk is taken to be horizontal; (ii) the flow is assumed to be axisymmetric; (iii) Coriolis forces are neglected; and (iv) v_θ is taken to be equal to ωr. The balance equations can then be reduced to the following two-dimensional system of equations in cylindrical coordinates:

$$\frac{1}{r}\frac{\partial}{\partial r}(rv_r)+\frac{\partial v_z}{\partial z}=0, \tag{8}$$

$$\rho\left(\frac{\partial v_r}{\partial t}+v_r\frac{\partial v_r}{\partial r}+v_z\frac{\partial v_r}{\partial z}-\omega^2 r\right)=-\frac{\partial p}{\partial r}-\frac{1}{r}\frac{\partial}{\partial r}(r\tau_{rr})+\frac{\tau_{\theta\theta}}{r}-\frac{\partial\tau_{rz}}{\partial z}, \tag{9}$$

$$\rho\left(\frac{\partial v_z}{\partial t}+v_r\frac{\partial v_z}{\partial r}+v_z\frac{\partial v_z}{\partial z}\right)=-\frac{\partial p}{\partial z}-\frac{1}{r}\frac{\partial}{\partial r}(r\tau_{rz})-\frac{\partial\tau_{zz}}{\partial z}+\rho g, \tag{10}$$

$$\frac{\partial w_s}{\partial t}+v_r\frac{\partial w_s}{\partial r}+v_z\frac{\partial w_s}{\partial z}=\frac{1}{r}\frac{\partial}{\partial r}\left(rD\frac{\partial w_s}{\partial r}\right)+\frac{\partial}{\partial z}\left(D\frac{\partial w_s}{\partial z}\right), \tag{11}$$

while the stress components and second invariant become

$$\tau_{rr}=-2\eta\frac{\partial v_r}{\partial r},\quad \tau_{\theta\theta}=-2\eta\frac{v_r}{r},\quad \tau_{r\theta}=0, \tag{12}$$

$$\tau_{zz}=-2\eta\frac{\partial v_z}{\partial z},\quad \tau_{rz}=-\eta\left(\frac{\partial v_r}{\partial z}+\frac{\partial v_z}{\partial r}\right),\quad \tau_{z\theta}=0, \tag{13}$$

$$I_2=2\left[\left(\frac{\partial v_r}{\partial r}\right)^2+\left(\frac{v_r}{r}\right)^2+\left(\frac{\partial v_z}{\partial z}\right)^2\right]+\left(\frac{\partial v_r}{\partial z}+\frac{\partial v_z}{\partial r}\right)^2. \tag{14}$$

Before we attempt to solve this complicated system of equations, we will nondimensionalize in such a manner that an ordering analysis may be performed. By doing so, we hope to determine appropriate characteristic quantities and to simplify further the equations while retaining the essential physics of the problem. The procedure for accomplishing this is outlined in Lin and Segal[25] and consists of scaling each variable with the appropriate value such that the nondimensionalized variable is of order one. First- and higher-order derivatives involving quantities of order unity are themselves assumed to be approximately of order unity. In this way the relative importance of each term is determined from the remaining dimensionless groups. The problem at hand considers fluid flow in a thin film and is similar to the scaling development of flow equations for the growth of a boundary layer near a sharp edge.[26] The occurrence of a strong centrifugal force, however, changes the nature of the problem slightly as will become apparent below.

We start with the equations describing fluid flow by scaling each variable in the following manner:

$$\tilde{r}=\frac{r}{R},\quad \tilde{z}=\frac{z}{H_0},\quad \tilde{v}_r=\frac{v_r}{V},\quad \tilde{v}_z=\frac{v_z}{U},$$

$$\tilde{\eta}=\frac{\eta}{\eta_0},\quad \tilde{p}=\frac{p-p_a}{\rho\omega^2H_0^2-p_a},\quad \tilde{t}=\frac{tV}{R}, \tag{15}$$

where the tilde identifies a dimensionless quantity, η_0 is the characteristic viscosity taken to be the value at the initial solvent concentration, R is the radius of the rotating disk, and p_a is the atmospheric pressure set arbitrarily to zero. U and V are not immediately obvious, hence they need to be determined from the problem itself. The characteristic value for the pressure, $\rho\omega^2H_0^2$, is chosen so that the pressure term remains of equal importance as the viscous terms in the axial momentum equation. There is some theoretical basis for this choice as Higgins[27] has shown that there must be a first-order pressure term in the classical axial momentum equation. H_0 is chosen as the initial characteristic axial space variable since it is the most obvious quantity. However, we note that this must be a maximum value and dictates the search for a more appropriate choice.

The continuity equation can be scaled to determine a relationship between the characteristic velocities. The resulting expression, $V/R \sim U/H_0$, is a statement of conservation of mass. Next we turn to the radial momentum equation to obtain a value for V. The centrifugal force is the main driving force for the fluid flow while the viscous resistance keeps the fluid from being flung completely from the disk. It is exactly when these two forces are competing that the spin-off stage is occurring. Therefore, a balance between these forces yields an estimate for the characteristic radial velocity of the fluid:

$$V\sim(\rho\omega^2RH_0^2)/\eta_0. \tag{16}$$

Finally, we can make one obvious simplification by realizing that the film is thin so that $H_0 \ll R$. Any term premultiplied by $(H_0/R)^2$ can therefore be neglected when compared to unity. With these choices in mind, we can simplify our system of differential equations to the following dimensionless form:

$$\frac{1}{\tilde{r}}\frac{\partial}{\partial\tilde{r}}(\tilde{r}\tilde{v}_r)+\frac{\partial\tilde{v}_z}{\partial\tilde{z}}=0, \tag{17}$$

$$\mathrm{Re}_0\left(\frac{\partial\tilde{v}_r}{\partial\tilde{t}}+\tilde{v}_r\frac{\partial\tilde{v}_r}{\partial\tilde{r}}+\tilde{v}_z\frac{\partial\tilde{v}_r}{\partial\tilde{z}}\right)-\tilde{r}=\frac{\partial}{\partial\tilde{z}}\left(\tilde{\eta}\frac{\partial\tilde{v}_r}{\partial\tilde{z}}\right), \tag{18}$$

$$\mathrm{Re}_0\left(\frac{\partial\tilde{v}_z}{\partial\tilde{t}}+\tilde{v}_r\frac{\partial\tilde{v}_z}{\partial\tilde{r}}+\tilde{v}_z\frac{\partial\tilde{v}_z}{\partial\tilde{z}}\right)=\frac{-\partial\tilde{p}}{\partial\tilde{z}}+\frac{\partial}{\tilde{r}\partial\tilde{r}}\left(\tilde{r}\tilde{\eta}\frac{\partial\tilde{v}_r}{\partial\tilde{z}}\right)+2\frac{\partial}{\partial\tilde{z}}\left(\tilde{\eta}\frac{\partial\tilde{v}_z}{\partial\tilde{z}}\right)+\mathrm{St}_0, \tag{19}$$

$$\tilde{\eta}=\tilde{\eta}_f(w_s)\left[1+\mathrm{De}_0\left(\frac{\partial\tilde{v}_r}{\partial\tilde{z}}\right)^2\right]^{(n-1)/2}, \tag{20}$$

where we have defined the following dimensionless quantities:

$$\mathrm{Re}_0=\frac{\rho^2\omega^2H_0^4}{\eta_0^2},\quad \mathrm{St}_0=\frac{g}{\omega^2H_0^4},\quad \mathrm{De}_0=\left(\frac{\rho\lambda\omega^2RH_0}{\eta_0}\right)^2. \tag{21}$$

Re_0 is the dimensionless Reynolds number, which describes the importance of the inertial forces to the viscous forces, St_0 is the Stanton number and describes the relative importance of the gravitational forces to the centrifugal forces, and De_0 is a type of Deborah number, which determines whether shear thinning is important. The subscript 0 indicates that these values are based on the initial conditions.

Next we scale the convective diffusion equation. The characteristic quantities are similar to Eq. (15) except that a new dimensionless time H_0^2/D_0 is defined because diffusion takes place on a different time scale than the fluid convection. D_0 is the characteristic diffusivity value based on the initial solvent concentration. Using these definitions and eliminating terms of order $(H_0/R)^2$ we derive the following dimensionless equation:

$$\frac{\partial w_s}{\partial\tilde{t}}+\mathrm{Pe}_0\left(\tilde{v}_r\frac{\partial w_s}{\partial\tilde{r}}+\tilde{v}_z\frac{\partial w_s}{\partial\tilde{z}}\right)=\frac{\partial}{\partial\tilde{z}}\left(\tilde{D}\frac{\partial w_s}{\partial\tilde{z}}\right), \tag{22}$$

where Pe_0 is the initial Peclet number defined as

$$\mathrm{Pe}_0=(\rho\omega^2H_0^4)/(\eta_0D_0), \tag{23}$$

and measures the importance of the convective terms to the mass transport of solvent.

Any system of differential equations requires appropriate initial and boundary conditions for the problem to be fully defined. We assume that initially a uniform film of known thickness rotates at the speed of the disk with a

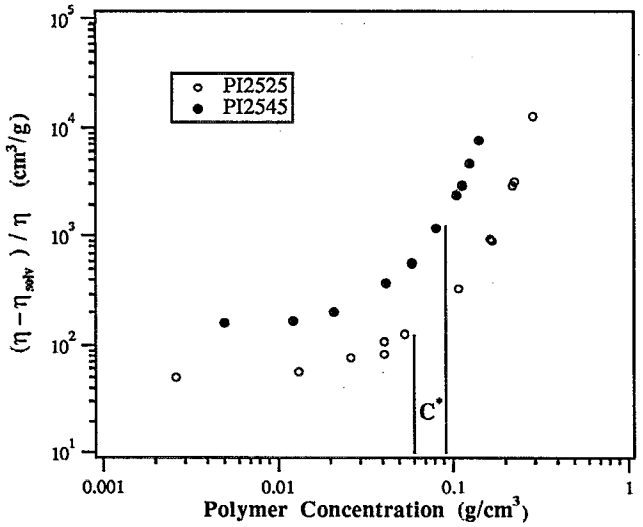

FIG. 2. Plot of the specific viscosity of two Du Pont polyimide precursor solutions as a function of polymer concentration. Entangled and semidilute regions for polyimide precursor solutions can be separated by a critical concentration C^*, which is 0.06 and 0.09 g/cm^3 for PI2525 and PI2545, respectively.

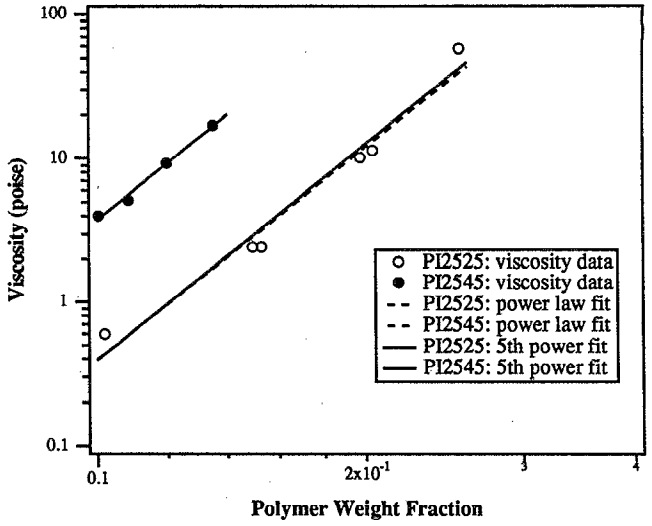

FIG. 3. Correlation of viscosity data by two different power-law expressions. The dotted curves were calculated based on a fit of the data to a power-law expression. For the solid lines, the power was fixed at 5. There is no apparent difference between the two fitting expressions.

uniform solvent concentration equal to that of the dispensing solution. At the solid substrate we impose the no-slip and no-solvent flux boundary conditions, essentially $v_r = 0$, $v_z = 0$, $v_\theta = \omega r$, and $\partial w_s/\partial z = 0$. At the free surface we impose a series of balance equations. The first,

$$\mathbf{n}\cdot(\mathbf{v}_{FS}-\mathbf{v})+(\dot{m}/\rho)=0, \tag{24}$$

is the so-called kinematic condition which is a statement of conservation of mass at the free surface. $\mathbf{v}_{FS}$ is the velocity of the free surface rather than the velocity of the fluid at the free surface $\mathbf{v}$, and $\mathbf{n}$ is the normal vector to the free surface. When the free surface is defined to be a function of only one of the coordinates, i.e., $h=f(r)$, the free-surface velocity $\mathbf{v}_{FS}$ has only an axial component and is equal to $\partial h/\partial t$.

The second term in this equation takes into account the mass flux at the free surface and is calculated using the following definition for the mass transfer coefficient:

$$\dot{m}=\dot{m}_s=\rho k(w_s^{g*}-w_{s\infty}^{g}), \tag{25}$$

where the superscript g indicates that these are gas-phase values and the asterisk represents that this value is in equilibrium with the solvent in the film at the free surface. The kinematic equation tracks the position of the free surface and therefore needs to be solved simultaneously with the other conservation equations. The nondimensional form of this expression becomes

$$\frac{\partial\tilde{h}}{\partial\tilde{t}}+\tilde{v}_r\frac{\partial\tilde{h}}{\partial\tilde{r}}-\tilde{v}_z+\frac{\mathrm{Sh}_0}{\mathrm{Pe}_0}(w_s^{g*}-w_{s\infty}^{g})=0, \tag{26}$$

where Sh_0 equals kH_0/D_0 and determines the relative importance of internal to external resistance to mass transfer.

We also enforce a balance of both stress and solvent mass at the free surface resulting in the following expressions:

$$-(p+\tau)\cdot\mathbf{n}=\gamma\left(\frac{1}{R_1}+\frac{1}{R_2}\right)\mathbf{n}-(p+\tau)_{\mathrm{air}}\cdot\mathbf{n}, \tag{27}$$

$$\mathbf{n}\cdot[(\mathbf{v}_{FS}-\mathbf{v})w_s+D\nabla w_s]+(\dot{m}_s/\rho)=0. \tag{28}$$

The subscript "air" indicates that this is the stress induced on the film surface by the overlying atmosphere, R_1 and R_2 are the principal radii of curvature of the free surface, and γ is the value of the surface tension coefficient at the film-air interface. The first equation is known as the Laplace equation and we can think of the second as a solvent kinematic condition that, using Eq. (24), can be transformed into

$$\mathbf{n}\cdot D\nabla w_s+(1-w_s)(\dot{m}_s/\rho)=0. \tag{29}$$

The Laplace equation can then be written in its dimensionless component form as

$$\tilde{\eta}\frac{\partial\tilde{v}_r}{\partial\tilde{z}}\tilde{n}_z=\frac{H_0^2}{\mathrm{Ca}\,R^2}\left(\frac{\partial^2\tilde{h}}{\partial\tilde{r}^2}+\frac{1}{\tilde{r}}\frac{\partial\tilde{h}}{\partial\tilde{r}}\right)\tilde{n}_r+\frac{(\mathbf{n}\cdot\sigma_{\mathrm{air}})_r}{\rho\omega^2H_0R}, \tag{30}$$

$$\tilde{\eta}\frac{\partial\tilde{v}_r}{\partial\tilde{z}}\tilde{n}_r+\left(2\tilde{\eta}\frac{\partial\tilde{v}_z}{\partial\tilde{z}}-\tilde{p}\right)\tilde{n}_z=\frac{1}{\mathrm{Ca}}\left(\frac{\partial^2\tilde{h}}{\partial\tilde{r}^2}+\frac{1}{\tilde{r}}\frac{\partial\tilde{h}}{\partial\tilde{r}}\right)\tilde{n}_z+\frac{(\mathbf{n}\cdot\sigma_{\mathrm{air}})_z}{\rho\omega^2H_0^2}. \tag{31}$$

Here terms of order H_0^2/R^2 were again neglected when compared with unity and we have defined

$$\mathrm{Ca}=\gamma/(\rho\omega^2R^2H_0) \tag{32}$$

as the capillary number, which is an indicator of whether surface tension forces are important. Similarly, the solvent kinematic condition can be nondimensionalized to obtain

$$\tilde{D}\frac{\partial w_s}{\partial\tilde{z}}\tilde{n}_z=-\mathrm{Sh}_0(1-w_s)(w_s^{g*}-w_{s\infty}^{g}). \tag{33}$$

We need to determine the mass transfer coefficient relevant to the spin-coating situation. Sparrow and Gregg[28]

and Krieth, Taylor, and Chong[29] have proposed the following correlation to calculate the mass transfer coefficient from a rotating disk to an infinite atmosphere:

$$\dot{m}_g = k_g(\rho_s^{g*} - \rho_{s\infty}^g). \tag{34}$$

For laminar flow, $\omega r^2/\nu_{\text{air}} < 2 \times 10^5$, these authors found the following expression to hold:

$$k_g = CD_a(\omega/\nu_{\text{air}})^{1/2}, \tag{35}$$

where D_a is the diffusivity of the solvent in the atmosphere and C is a constant that depends on the dimensionless quantity $\text{Sc}_a = \nu_{\text{air}}/D_a$.[29] Note that the mass transfer coefficient is independent of radial position and depends only on the ambient conditions and the square root of the rotational speed. Since the gas phase is very dilute in solvent, we replace the solvent gas-phase density ρ_s^g by the product of the air density and the gas phase solvent weight fraction. Comparison to the model definition for the mass transfer coefficient, Eq. (25), results in the following expression:

$$k = CD_a(\rho_{\text{air}}/\rho)(\omega/\nu_{\text{air}})^{1/2}. \tag{36}$$

The weight fraction of solvent in the gas phase in equilibrium with the surface weight fraction in the film is also required. Therefore we need an expression, a so-called equation of state, relating the solvent weight fractions in the solution to the gas state above it. The Flory–Huggins equation[30] is the simplest and most common of these equations and gives a reasonable representation of the behavior especially when the volume fraction of polymer is above its critical entanglement point. Using the ideal gas law to describe the gas-phase behavior and replacing volume fractions with weight fractions, we can rearrange the Flory–Huggins expression to the following form:

$$w_s^{g*} = \frac{M_s P^{\text{sat}}}{RT\rho_{\text{air}}} w_s \exp[(1-w_s)+\chi(1-w_s)^2] = \Phi(w_s)w_s, \tag{37}$$

where M_s is the molecular weight of the solvent, P^{sat} is the pure component solvent vapor pressure, R is the universal gas constant, and T is temperature. Φ can be thought of as a Henry's coefficient with an exponential correction term that is of order unity, and χ is referred to as the Flory interaction parameter and is a measure of the interaction between the polymer and the solvent.

E. Ordering arguments

Equations (17)–(20), (22), and (26) along with the boundary conditions [Eq. (30), (31), and (33)] comprise the most general model of the spin-coating process. However, one of the above-mentioned goals for nondimensionalizing the system of equations was to perform an ordering analysis. We have already used one simple scaling concept which was the thin-film approximation to neglected terms of order $(H_0/R)^2$ when compared to unity. The problem can be further simplified based on the typical spinning conditions put forth in Table I. The Reynolds number takes on values between 4×10^{-8} and 7×10^{-3} when H_0 is 100 μm. For larger values of film thickness the centrifugal force would clearly dominate and we would still be in the spin-up stage. As the characteristic film thickness decreases or spinning continues, the Reynolds number diminishes further. Therefore, the inertial terms are clearly not important when modeling spin coating on a flat horizontal plate. Taking typical values for surface tension (30 dyn/cm) and disk radius (5 cm), it is possible to calculate 10^{-3} and 10^{-8} for (1/Ca) and $(H_0^2/\text{Ca}\,R^2)$, respectively. Hence, the effects of surface tension may also be neglected.

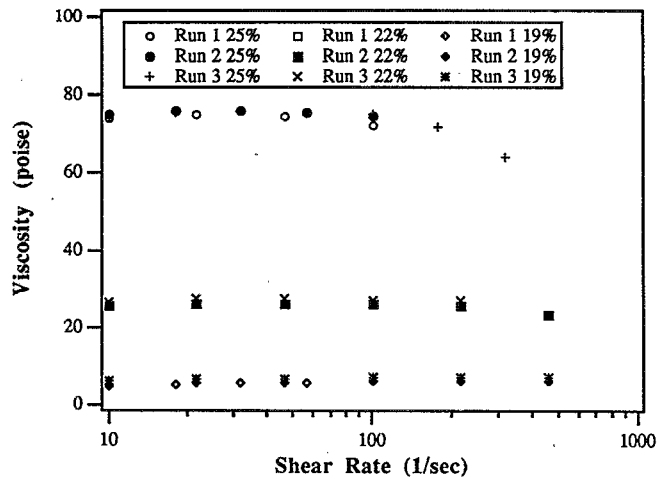

FIG. 4. Shear rate dependence of Du Pont PI2525 viscosity at 22 °C. Weight % values given in the legend are rounded off. The viscosity appears to be nonshear thinning over this range of shear rates and the reproducibility of the experimental technique appears quite good.

Based on the definition of the Deborah number De_0 the possibility of shear thinning can be neglected when the relaxation constant λ is less than 0.01 s. An experimental study of two polyimide precursor solutions showed no significant shear thinning below 100 rad/s (see Fig. 4). Further, Jenekhe[31] has investigated the rheology of similar polyimide precursor solutions and found that the onset of shear thinning behavior was in the range of 30–440/s. Therefore, at least for these polyimides, the solutions may be treated as simple Newtonian fluids and the possibility of shear thinning may be neglected.

In contrast to the above dimensionless numbers, the Peclet and Sherwood numbers may change orders of magnitude during the spin coating process. Even the initial values may vary greatly depending on the specific cases. Therefore all the terms in the mass transfer equations must be included until a better characteristic film thickness is determined.

With these simplifications in mind, the system of equations becomes

$$\tilde{r} + \frac{\partial}{\partial \tilde{z}}\left(\tilde{\eta}\frac{\partial \tilde{v}_r}{\partial \tilde{z}}\right) = 0, \tag{38}$$

$$-\frac{\partial \tilde{p}}{\partial \tilde{z}} + \frac{1}{\tilde{r}}\frac{\partial}{\partial \tilde{r}}\left(\tilde{r}\tilde{\eta}\frac{\partial \tilde{v}_r}{\partial \tilde{z}}\right) + 2\frac{\partial}{\partial \tilde{z}}\left(\tilde{\eta}\frac{\partial \tilde{v}_z}{\partial \tilde{z}}\right) + \text{St}_0 = 0, \tag{39}$$

$$\tilde{\eta} = \tilde{\eta}_r(w_s), \tag{40}$$

$$\frac{\partial w_s}{\partial \tilde{t}}+\mathrm{Pe}_0\left(\tilde{v}_r\frac{\partial w_s}{\partial \tilde{r}}+\tilde{v}_z\frac{\partial w_s}{\partial \tilde{z}}\right)=\frac{\partial}{\partial \tilde{z}}\left(\tilde{D}\frac{\partial w_s}{\partial \tilde{z}}\right), \tag{41}$$

$$\frac{\partial \tilde{h}}{\partial \tilde{t}}+\tilde{v}_r\frac{\partial \tilde{h}}{\partial \tilde{r}}-\tilde{v}_z+\frac{\mathrm{Sh}_0}{\mathrm{Pe}_0}(w_s^{g^*}-w_{s\infty}^g)=0, \tag{42}$$

and the free-surface boundary conditions become

$$\tilde{\eta}\frac{\partial \tilde{v}_r}{\partial \tilde{z}}\tilde{n}_z=\frac{(\mathbf{n}\cdot\sigma_{\mathrm{air}})_r}{\rho\omega^2 H_0 R}, \tag{43}$$

$$\tilde{\eta}\frac{\partial \tilde{v}_r}{\partial \tilde{z}}\tilde{n}_r+\left(2\tilde{\eta}\frac{\partial \tilde{v}_z}{\partial \tilde{z}}-\tilde{p}\right)\tilde{n}_z=\frac{(\mathbf{n}\cdot\sigma_{\mathrm{air}})_z}{\rho\omega^2 H_0^2}, \tag{44}$$

$$\tilde{D}\frac{\partial w_s}{\partial \tilde{z}}\tilde{n}_z=-\mathrm{Sh}_0(1-w_s)(w_s^{g^*}-w_{s\infty}^g), \tag{45}$$

while the solid surface boundary conditions remain

$$\tilde{v}_r=0,\quad \tilde{v}_z=0,\quad \frac{\partial w_s}{\partial \tilde{z}}=0. \tag{46}$$

IV. ONE-DIMENSIONAL MODEL OF SPIN COATING

Equations (38)–(46) comprise a complete set necessary to describe the spin-coating problem. They have been simplified while retaining the physics necessary to study most relevant aspects of the problem. For example, the effect of the environment such as forced air flow past the disk or a partial pressure of solvent in the atmosphere could be investigated. Also, mechanistic details such as the leveling of nonuniform film thickness may be studied. These problems are deferred for a later study and a simpler version of these equations will be solved to answer the important question of the coupling between the mass transfer and fluid mechanics without including two-dimensional complications.

In this model we will further assume that the film remains uniform throughout the spin-off stage, thereby causing the dimensionless film thickness to be only time dependent. Earlier studies have shown that the final film thickness of spun-cast films tends to be of uniform thickness and that any nonuniformities are removed during spinning.[8,17] Consistent with this assumption, the solvent weight fraction will also be independent of radial position because the mass transfer coefficient is independent of position. Finally, in order for the film thickness to be independent of radial position we must require that the viscosity be independent of shear rate. A shear thinning viscosity would result in smaller shear forces at larger radial positions where the rate of shear is stronger. This would lead to a nonuniform film thickness. However, the assumption of no shear thinning was shown to be adequate for the polyimides of interest here. Finally, we neglect the effects of air shear, as those induced naturally by the rotating disk have been shown to be negligible except for film thickness much less than those found in microelectronics.[19,32]

With these additional assumptions in mind we simplify our equations following the approach used by Bornside and co-workers[14] to arrive at a set of one-dimensional integropartial differential equations. This set of equations will be derived from the dimensional form of Eqs. (38)–(46). First, the radial momentum equation is integrated twice to determine an expression for the radial velocity component,

$$v_r=\rho\omega^2 r\int_0^z\frac{(h-z')}{\eta}\,dz'. \tag{47}$$

Next, we substitute this expression into the continuity equation to obtain

$$\frac{\partial v_z}{\partial z}+2\rho\omega^2\int_0^z\frac{(h-z')}{\eta}\,dz'=0. \tag{48}$$

Since the solvent weight fraction is independent of radial position we can further simplify the solvent conservation equation to be

$$\frac{\partial w_s}{\partial t}+v_z\frac{\partial w_s}{\partial z}=\frac{\partial}{\partial z}\left(D\frac{\partial w_s}{\partial z}\right), \tag{49}$$

while the kinematic expression at the free surface is also simplified to

$$\frac{\partial h}{\partial t}-v_z+k(w_s^{g^*}-w_{s\infty}^g)=0. \tag{50}$$

Under the conditions specified, the boundary conditions become

$$v_z=0,\quad \frac{\partial w_s}{\partial z}=0,\quad \text{at } z=0, \tag{51}$$

and

$$D\frac{\partial w_s}{\partial z}=-k(1-w_s)(w_s^{g^*}-w_{s\infty}^g),\quad \text{at } z=h. \tag{52}$$

A. Characteristic film thickness

The initial value is not an appropriate characteristic quantity for film thickness because the final spin-coated film thickness has been shown to be independent of this value. Therefore, the initial Peclet and Sherwood numbers are not representative of the nature of the mass transfer. Recall (Fig. 1) that initially the loss of film height is dominated by the fluid convection, and then mass transfer becomes competitive and eventually controls the film thinning process. The film thickness where the two mechanisms become of equal importance would be the most appropriate value for the characteristic film thickness. At values larger than this, film thinning is controlled almost exclusively by fluid convection and mass transfer is unimportant. Only when the film has thinned to where solvent evaporation begins to compete for film thinning does the process begin to deviate from the classical solution by Emslie and co-workers.[8] It is this critical influence of the mass transfer that eventually set the final film thickness. Stated in an equivalent manner, the characteristic film thickness H should be chosen such that the mass transfer and fluid convection terms are of equal order of magnitude in the scaled kinematic condition, Eq. (42). Therefore we require that

$$\frac{\mathrm{Sh}}{\mathrm{Pe}}=\frac{k\Phi(w_{s0})\eta_0}{\rho\omega^2H^3}\equiv 1 \quad \text{or} \quad H=\left(\frac{k\Phi(w_{s0})\eta_0}{\rho\omega^2}\right)^{1/3}. \tag{53}$$

Based on this characteristic film thickness we can begin to examine two regimes for the mass transfer properties. The first is where the solvent mass transfer is controlled by the external mass transfer coefficient. This corresponds to a small value of the Sherwood number Sh. Here the diffusion coefficient is essentially infinite and the solvent concentration is constant across the film. We solved this simplified model as a test to the more elaborate model where both external and internal resistances to mass transfer occur. The extreme case of negligible external mass transfer resistance is not considered separately, but as part of the second, more elaborate model. For this situation the diffusivity values are likely to be so low that a solid film of polymer would grow at the free surface and the spin-coating process would likely be unsuccessful. Bornside and co-workers[14] have considered this special problem and we will not study it as a separate case.

B. Externally controlled mass transfer model

For this situation the internal diffusive resistance is assumed negligible and the solvent weight fraction can be taken as a constant. Since there are no solvent gradients, the viscosity is no longer a function of position, and the flow equations, Eqs. (47) and (48), can be integrated directly to give

$$v_r=\frac{\rho\omega^2 r}{\eta}(hz-z^2) \quad \text{and} \quad v_z=-\frac{\rho\omega^2}{\eta}\left(hz^2-\frac{1}{3}z^3\right). \tag{54}$$

These are equivalent in form to the classical solution of Emslie and co-workers,[8] except here the viscosity is a function of time by virtue of the changing solvent weight fraction. The kinematic condition can also be stated in a more explicit form in light of these simplifications, namely,

$$\frac{dh}{dt}=-\frac{\rho\omega^2}{\eta}h^3-k(w_s^{g*}-w_{s\infty}^g). \tag{55}$$

In addition, we require a solvent mass balance in order to track its weight fraction in the film,

$$\frac{dw_s}{dt}=-\frac{k}{h}(1-w_s)(w_s^{g*}-w_{s\infty}^g). \tag{56}$$

These two coupled ordinary differential equations, in conjunction with a relationship for the viscosity dependence on solvent weight fraction, can then be solved simultaneously to obtain the time dependence of the film thickness.

C. Numerical flashing

After spin coating, the film is typically subjected to a baking stage to remove any remaining solvent. The result is a film of pure polymer. Once solvent mass transfer has dominated the film thinning process, we can ignore fluid convection and only consider solvent mass transfer. Since the final film thickness is the ultimate desired quantity, a simplification may be introduced where all remaining solvent is immediately removed leaving a solid polymer film behind. We will term this procedure flashing and note that it is only a mathematical simplification and does not physically occur. A simple mass balance results in the following expression for the final film thickness,

$$h_f=\int_0^h (1-w_s)\,dz. \tag{57}$$

D. Split mechanism model

In order to compare the exact results obtained by considering mass transfer during the entire spin-coating process to those obtained by separating the two mechanisms, we must determine the procedure for the latter approximate model, which we term the split mechanism model. This simple model assumes that the film is thinned first by fluid convection alone and then exclusively by mass transfer. The transition between these two processes takes place when the rate of film thinning by each would be equal. Referring to the kinematic expression, Eq. (50), we see that the condition for this change over of mechanisms is given by

$$-v_z=k[\Phi(w_{s0})w_{s0}-w_{s\infty}^g], \tag{58}$$

where the variables are evaluated at the free surface.

The first part of the spin-off stage consists of fluid flow without solvent evaporation and the expression for the film thickness as a function of time,

$$h=\frac{H_0}{\sqrt{(4\rho\omega^2H_0^2t/3\eta_0)+1}}, \tag{59}$$

is just the classical expression first derived by Emslie and co-workers for a Newtonian fluid without solvent evaporation.[8] Based on Eq. (58) it is then possible to solve for the value of the film thickness h^* at which this arbitrary transfer of mechanisms would take place,

$$h^*=\sqrt[1/3]{\frac{3k\eta_0[\Phi(w_{s0})w_{s0}-w_{s\infty}^g]}{2\rho\omega^2}}. \tag{60}$$

The time at which this transition of mechanisms occurs may also be determined,

$$t^*=\frac{3\eta}{4\rho\omega^2H_0^2}\left(\sqrt[2/3]{\frac{2\rho\omega^2H_0^3}{3k\eta_0[\Phi(w_{s0})w_{s0}-w_{s\infty}^g]}}-1\right). \tag{61}$$

Note that the dependence on H_0 cancels for most cases as the root term is much larger than unity. After this time we assume that the solvent evaporation mechanism dominates. Since only the final film thickness is required, we can use the flashing technique discussed above to remove the solvent. In this case the solvent weight fraction is uniform throughout the film after t^* and the final film thickness becomes

$$h_f=h^*(1-w_{s0}). \tag{62}$$

V. SOLUTION TECHNIQUE

The procedure for solving this system of nonlinear differential equations is based on a Galerkin finite element method over deforming elements combined with a finite difference predictor-corrector scheme for the temporal integrations. It follows a scheme outlined by Keunings[33] for simulating transient viscoelastic flows with free surfaces, however, in a much simplified form. The free-surface displacement is unknown *a priori* and is determined simultaneously with the flow and concentration fields. The grid is then deformed to follow the motion of the free surface and grid motion is incorporated in the formulation of the discretized finite element problem.

The finite element method is a powerful technique for solving difficult differential equations in complex geometries. Strang and Fix[34] and Reddy[35] discussed the finite element method in detail, while an introduction to the subject can be found in several texts (for example, Reddy[36]). The finite element technique reduces the problem to a set of algebraic equations that are then solved using linear algebraic methods.

VI. PHYSICAL PARAMETERS FOR SPIN-COATING MODEL

In order to compare the model prediction to experimental data, it is necessary to determine the physical parameters for the spin-coating model. In general, very few data are available for polyimide precursor solutions and the N-methyl-2-pyrrolidinone solvent. Whenever possible, measurements were made to determine the most accurate value for the parameters. If this was not possible then estimates were made based on theoretical and empirical relationships. The paragraphs below discuss the best method utilized to determine these physical parameters.

A. Viscosity coefficients

The viscosity of two Du Pont polyimide precursor solutions, PI2525 and PI2545, was measured using two separate methods. First, the concentration dependence of the viscosity coefficient η_0 was investigated using bulb viscometry. An Ostwald no. 0C viscometer was utilized for the lower-viscosity measurements, while a Cannon–Fenske no. 300 viscometer was used for the high-viscosity solutions. The concentration range of interest for the spin-coating process is one that starts with the stock solution and becomes more concentrated in polymer. However, it is extremely difficult to form more concentrated polymer solutions as the vapor pressure of the NMP solvent is extremely low at room temperature, approximately 4 Torr.[37] Further, it is well known that the polyimide precursor, polyamic acid, reacts slowly at room temperature.[38] This premature conversion would result in a stiffer chain thereby changing the rheological properties of the solution. Elevating the temperature to remove solvent would also not work as this would facilitate the reaction. It is therefore necessary to extrapolate diluted solution data to higher concentrations in the most intelligent manner possible.

Polymer solutions can exist in two different states. In the so-called semidilute regime the polymer molecules behave as isolated chains in a roughly spherical orientation with little interaction. At some higher concentration C^* these isolated "spheres" begin to overlap and the polymer chains interact with one another. Above this concentration the chains are in an entangled state and the viscosity often follows an empirical rule,

$$\eta \sim c^a, \tag{63}$$

where a is typically equal to 5.[39] Figure 2 illustrates the semidilute and entangled regimes of these solutions where C^* is approximately 0.09 g/cm^3 for PI2525 and 0.06 g/cm^3 for PI2545. This corresponds to 8.6 and 5.8 wt % polymer for PI2525 and PI2545, respectively. Since the entire spin-coating process takes place in the entangled region, the data greater than C^* were fitted to a power-law relationship between viscosity and weight fraction. The resulting expressions are

$$\eta_{\mathrm{PI2525}} = 3.254 \times 10^4 (1 - w_s)^{4.918}, \tag{64}$$

$$\eta_{\mathrm{PI2545}} = 3.927 \times 10^5 (1 - w_s)^{5.028}, \tag{65}$$

where the viscosity coefficient is measured in units of poise. Since the power exponent in each expression is very close to empirical value of 5, one is tempted to use this value and take an average value for the prefactor. This alternate approach leads to the following equations:

$$\eta_{\mathrm{PI2525}} = 3.89 \times 10^4 (1 - w_s)^5, \tag{66}$$

$$\eta_{\mathrm{PI2545}} = 3.70 \times 10^5 (1 - w_s)^5. \tag{67}$$

Figure 3 compares these expressions both to the first expressions and to the experimental data. The dotted lines correspond to Eqs. (64) and (65), while the solid lines refer to values calculated using Eqs. (66) and (67). There is essentially no difference between the values predicted by the two alternative expressions and the fit to the experimental data is excellent. Therefore, the simpler fifth-power expressions, Eqs. (66) and (67), will be chosen as the viscosity relationships.

The shear thinning nature of the fluid was tested using a RMS-705 rheometer by Rheometrics with a 12.5-mm-radius plate and a 5° cone. The cone and plate geometry was chosen because the shear field is constant throughout the fluid. Several weight fractions in the entangled regime were tested. However, the range of shear rates was limited by the measurable torque of the transducer and the tendency of the fluid to be flung from the disk at high rotational speeds. Figure 4 shows the results of these experiments for three different weight fractions. There appears to be no effect of shear thinning except for possibly the ~25 wt % polymer solution when the shear rate was above 100/s. However, for this range of shear rates the torque on the transducer is approaching its limiting range and the viscosity is dropping off because the reading at the transducer is no longer accurate.

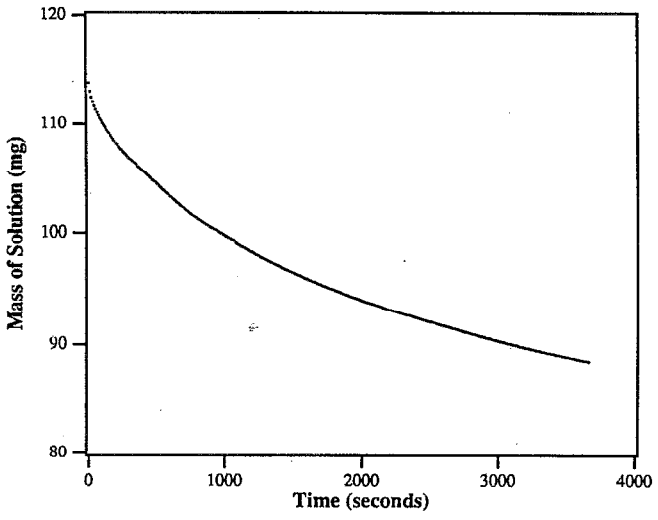

FIG. 5. Desorption of solvent at vacuum at 25 °C from Du Pont PI2525 precursor solution initially at 25.5 wt % polymer. Measurements were taken using a Cahn electrobalance.

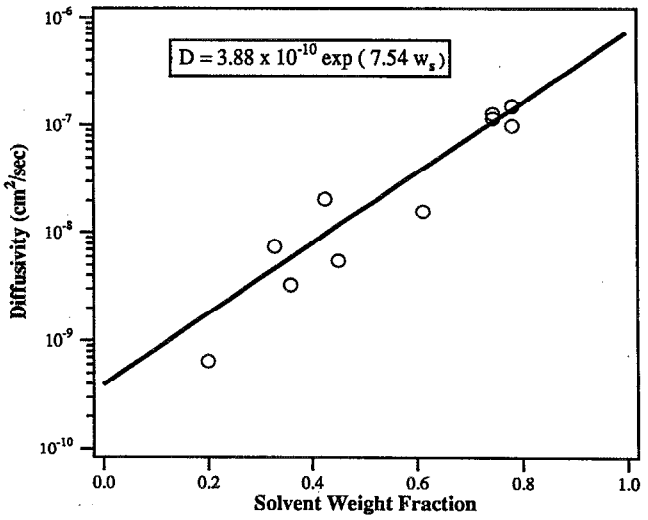

FIG. 6. Exponential fit of diffusion coefficient to solvent weight fraction. A simple exponential expression was chosen since the accuracy and scatter of the data does not warrant a more sophisticated expression.

B. Diffusion coefficients

The diffusivity data were taken using a model D200 digital recording balance by Cahn Instruments. This instrument converts the torque required to maintain a balance between the sample pan and a counterweight into sample weight. Further details about the operation of electrobalances can be found elsewhere.[40–42] Figure 5 illustrates the typical output from this balance for the desorption of solvent from a polyimide precursor solution. The desorption experiment was conducted under vacuum at 25 °C. The diffusion coefficient can be obtained from the initial data in Fig. 5. For short times the film can be assumed infinite in extent, thereby creating a classical similarity problem from which the following expression for the total mass as a function of time can be derived.[43]

$$M_t = M_0 - \frac{2A\rho w_{s0}\sqrt{D}}{\sqrt{\pi}}\sqrt{t}. \tag{68}$$

Here M is the mass of solution and A is the cross-sectional area. The diffusion coefficient, therefore, may be determined from the limiting slope of a plot of mass versus the square root of time. Since the diffusivity value is extracted from very short-time data, we may safely assume that the solvent weight fraction has not changed from its initial value.

An exponential form is chosen to fit the experimental data as it contains the essential features of the dependence of the diffusion coefficient on concentration and it is simple enough to be fitted by a limited amount of data. Although this will not predict the exact nature of the polymeric solution, it should provide the trends necessary for this model. Figure 6 illustrates the fit of the data to the following exponential expression:

$$D = 3.88\times 10^{-10}\exp(7.54 w_s), \tag{69}$$

where the diffusion coefficient is measured in cm^2/s.

Since there is no literature data available to assess if this expression is reasonable, we compare the dilute diffusivity value to that predicted from the simple Einstein equation,[44]

$$D = \frac{k_B T}{\eta_{\text{soln}}}\frac{1}{4\pi R_s}, \tag{70}$$

where k_B is the Boltzman constant, R_s is the effective radius of the solvent molecule and can be estimated from critical properties and group contribution methods to be 2.82 Å,[43] and η_{soln}, the solution viscosity, is taken to be 1 P. The typical diffusivity value of NMP in a reasonably dilute polyimide precursor solution is then estimated to be 10^{-7}. This is in excellent order-of-magnitude agreement with the experimental data.

C. Mass transfer coefficient

Both available and estimated data were combined to evaluate Eq. (36) for the mass transfer coefficient. At 25 °C, the density of air is found to be 0.0013 g/cm^3 and the kinematic viscosity of air ν_{air} can be calculated to be 0.1597 cm^2/s based on data obtained from Perry's Chemical Engineering Handbook.[45] The diffusivity of solvent (NMP) in air D_a can be estimated using the Chapman–Enskog theory for diffusion of gases[44] to be 0.075 cm^2/s. Hence, the following expression for the mass transfer coefficient can be derived:

$$k = 1.17\times 10^{-4}\omega^{1/2}\ (\text{cm/s}^{1/2}). \tag{71}$$

D. Equilibrium expression

The equilibrium expression based on the Flory–Huggins equation for polymeric solutions, Eq. (37), requires three additional physical parameters for polyimide precursor solutions. The solvent molecular weight is 99.13 g/mol and the vapor pressure is 4 Torr.[37] No data, how-

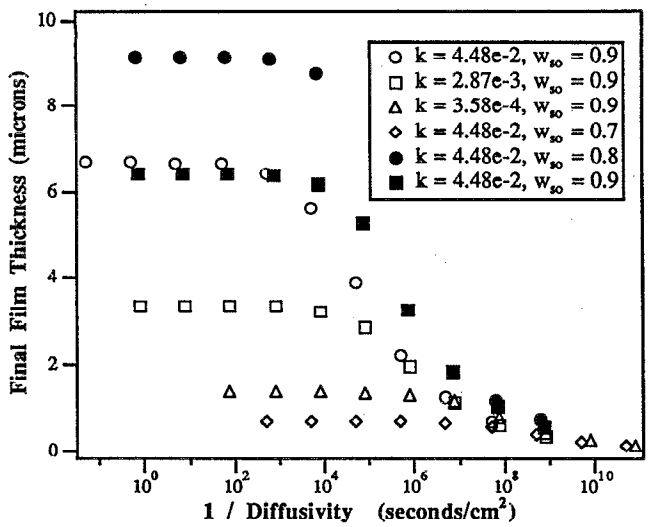

FIG. 7. Results of spin-coating model where the final film thickness is plotted against changing mass transfer properties.

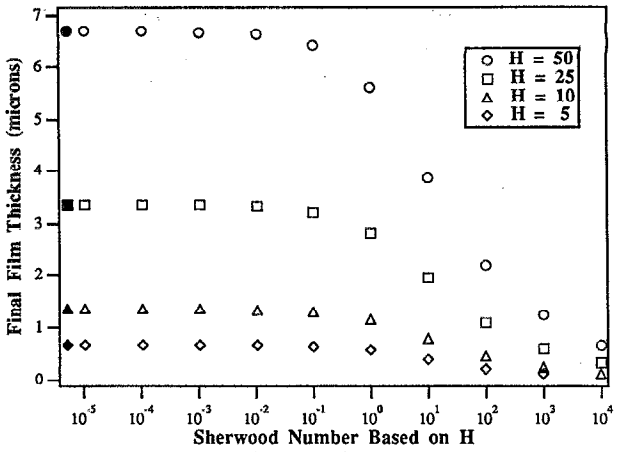

FIG. 8. The final film thickness predicted by the spin-coat model for fluid flow on a rotation disk. H is a characteristic length scale where the mass transfer effects become as important as the fluid convection for film thinning. The initial solvent weight fraction for each of these curves was 0.9. The Sherwood number is a measure of the relative importance of the external to internal mass transfer resistance at this characteristic film thickness. The solid symbols represent the limiting value when the mass transfer is controlled exclusively by the external mass transfer coefficient.

ever, exist for χ for this polymer-solvent combination and an approximate value of 0.1 is chosen because NMP is a good solvent for the polymer, yet the mixture should not be completely athermal. This choice is not crucial as the Flory–Huggins model is itself a crude approximation of polymeric solution behavior. Also, the correction term containing χ is of order unity and does not influence the model results to any large extent. Based on these values, the room-temperature liquid-vapor equilibrium coefficient in Eq. (37) becomes

$$\Phi(w_s)=0.016\exp[(1-w_s)+0.1(1-w_s)^2]. \tag{72}$$

VII. RESULTS AND DISCUSSION

Figure 7 shows the final film thickness predicted by various combinations of the initial solvent weight fraction and mass transfer parameters. Obviously this representation is too complicated to extract any useful information about spin coating. Similarly, plotting a series of curves changing a few parameters while holding others constant does not offer fundamental understanding of the spin-coating process. Therefore, we are interested in presenting the data in such a manner that it is possible to gain insight into the physics of the problem and possibly to find universal predictive capabilities. With these goals in mind we plot the data as functions of characteristic parameters determined from our scaling analysis.

Figure 8 shows the final film thickness predicted for various values of the characteristic film thickness, H and Sherwood number Sh. Notice that at small values of Sh, the final film thickness is relatively independent of this parameter. In fact, the final film thicknesses predicted by the exact model converge to limit the value predicted when Sh is set to zero (placed arbitrarily at $\mathrm{Sh} = 5\times10^{-6}$). This is the externally controlled model discussed above, Eqs. (55) and (56), where the mass transfer is controlled exclusively by the external mass transfer resistance and the solvent weight fraction was constant across the film.

For intermediate values of the Sherwood number, the final film thickness begins to drop off with increasing Sh. The fact that this change begins to occur on the order of unity justifies the choices made for the characteristic values during scaling. It is in this region that both external and internal resistances to mass transfer are important. Notice that at larger values of the Sherwood number, the final film thickness again seems to be independent of Sh. These values are at the fringe of stability in the convective diffusion equation and it is difficult to obtain points at larger values of Sh. However, the data suggest that we are entering a region where the external mass transfer resistance is negligible and the concentration profiles are determined exclusively by the diffusivity.

If the predicted final film thicknesses are divided by the corresponding characteristic film thickness H and plotted against Sh, all four curves collapse to one. However, separate dimensionless curves result for a different initial film solvent weight fraction. In order to understand and justify this collapse of the data and to determine the best method of further superimposing the data, we take a closer look at the scaling and nondimensionalization of the model equations. First, the following scaling variables are defined:

$$\tilde{z}=\frac{z}{H_c},\quad \tilde{h}=\frac{h}{H_c},\quad \tilde{v}_z=\frac{v_z}{U}=\frac{\eta_0 v_z}{\rho\omega^2 H_c^3},$$

$$\tilde{t}_D=\frac{tD_0}{H_c^2},\quad \tilde{t}_H=\frac{tU}{H_c},\quad \theta_s=\frac{\Phi(w_s)w_s-w_{s\infty}^g}{\Phi(w_{s0})w_{s0}-w_{s\infty}^g}. \tag{73}$$

Previously Φ was included in the scaling arguments so that the appropriate order of magnitude could be determined; however, the inclusion of θ_s as a concentration variable handles the nondimensionalization in a more consistent manner. Again, two different time scales, t_D and t_H, are

used for scaling the convective diffusion equation and kinematic expression, respectively.

The result of this nondimensionalization of the model equations is

$$\partial\tilde{v}_z/\partial\tilde{z}+2\int_0^{\tilde{z}}\frac{(\tilde{h}-\tilde{z}')}{\tilde{\eta}}\,d\tilde{z}'=0, \tag{74}$$

$$\frac{\partial\theta_s}{\partial\tilde{t}}+\mathrm{Sh}_c\tilde{v}_z\frac{\partial\theta_s}{\partial\tilde{z}}=\frac{\partial}{\partial\tilde{z}}\left(\tilde{D}\frac{\partial\theta_s}{\partial\tilde{z}}\right), \tag{75}$$

$$\frac{\partial\tilde{h}}{\partial\tilde{t}}=\tilde{v}_z-\theta_s. \tag{76}$$

The characteristic value of the film thickness,

$$H_c=\left(\frac{k\eta_0[\Phi(w_{s0})w_{s0}-w_{s\infty}^g]}{\rho\omega^2}\right)^{1/3}, \tag{77}$$

was determined by requiring that all terms in the kinematic expression, Eq. (76), be of the same order of magnitude. H_c includes the mass transfer driving force through the addition of w_{s0} and $w_{s\infty}^g$. The characteristic Sherwood number is now defined as

$$\mathrm{Sh}_c=\frac{kH_c[\Phi(w_{s0})w_{s0}-w_{s\infty}^g]}{D_0}. \tag{78}$$

The boundary and initial conditions must also be nondimensionalized consistent with the above equations. The resulting expressions are

$$\tilde{D}\frac{\partial\theta_s}{\partial\tilde{z}}=-\mathrm{Sh}_c(\theta_1-\theta_s)\theta_s, \quad \text{at } \tilde{z}=\tilde{h},$$

$$\tilde{D}\frac{\partial\theta_s}{\partial\tilde{z}}=0, \quad \text{at } \tilde{z}=0, \quad \text{and} \quad \theta_s=1, \quad \text{at } \tilde{t}=0, \tag{79}$$

where θ_1 is

$$[\Phi(w_{s0})-w_{s\infty}^g]/[\Phi(w_{s0})w_{s0}-w_{s\infty}^g].$$

This system of equations has essentially two parameters, Sh_c and θ_1. At first it would be tempting to suggest that the parameter θ_1 is the cause of the deviation in the curves when the initial solvent weight fraction is changed. However, this parameter is always of order unity, and it does not play a significant role in determining h_f/H_c.

It is possible to collapse the entire set of data to one curve as illustrated by Fig. 9. This general curve is independent of physical parameters, spinning conditions, and initial solvent content. The $(1-w_{s0})$ factor accounts for the eventual removal of solvent that occurs upon drying the film. Note that what changes along the abscissa is the mass transfer properties of the polymer solvent system. When investigating a new polymer formulation or polymer-solvent combination, it is not necessary to perform new spin-coating experiments or repeat the model calculations. If the physical parameters of the coating solution and the spinning conditions are known then this general curve allows the prediction of film thickness. Also, the effect of changing various conditions, such as spinner

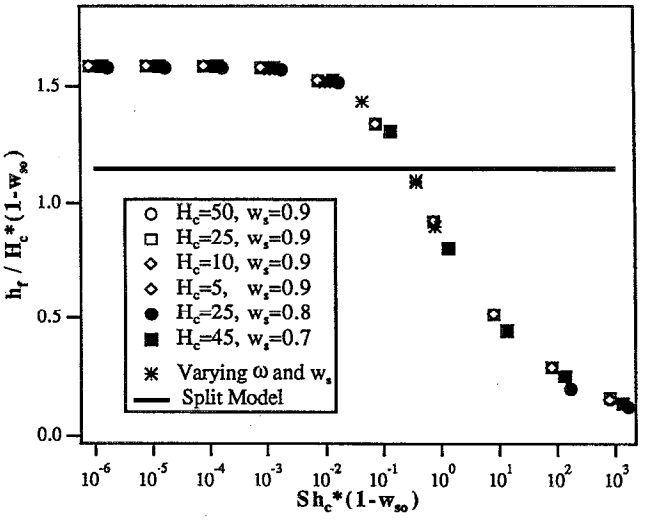

FIG. 9. When the final film thickness is scaled by dividing by the characteristic value of $H_c(1-w_{s0})$ and the Sherwood number is also based on this value then the entire set of data collapses to one curve. The solid line corresponds to the film thickness that would be predicted by the split mechanism model where the fluid convection and solvent evaporation are divided into two separate stages.

rotational speed discussed below, may be determined directly from this curve and the definitions of H_c and Sh_c.

Finally, we compare the split mechanism model (solid line in Fig. 9) to the values calculated from the complete model. This split model was developed earlier, and the major assumption is that the spin-coating process can be divided into two stages, one where fluid flow is occurring exclusively and the other where only mass transfer occurs. The approach does not allow for any dependence of the final film thickness on the diffusion coefficient. Figure 9 shows that significant error can occur by applying the simple split mechanism model, especially at larger values of the Sh_c. Attempts have been made to correct for this inaccuracy of the split mechanism model by allowing the time and/or the solvent content when this transition of mechanisms occurs to be determined experimentally. However, this reduces the model to an empirical fitting expression and is no longer predictive.

A. Comparison of model results to typical behavior

It is well documented that spin-coated films tend to follow a power-law dependence between the final film thickness and the rotational speed:

$$h_f\sim\omega^b. \tag{80}$$

Most investigators report a value of $-\frac{1}{2}$ for b,[2–5] while Daughton and Givens[5] reported a value of -0.8 for higher-viscosity liquids, specifically polyimides, and Lai[4] claimed that it depended on evaporation conditions. This dependence was investigated using the model equations and the physical parameters determined for our polyimides. Figure 10 shows the results of this investigation, a power-law dependence with the exponent being $-\frac{1}{2}$. In actuality Fig. 9 and the definitions for H_c and Sh_c, Eqs. (77) and (78), would yield the required information. The cor-

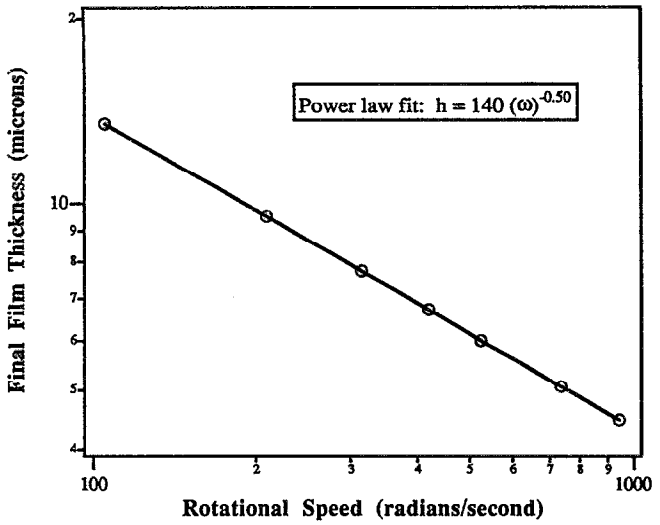

FIG. 10. A power-law dependence is predicted for the dependence of the final film thickness on the rotational speed. This final film thickness calculation assumed that spinning proceeded long enough for the solvent mass transfer to be the dominant mechanism of film thinning.

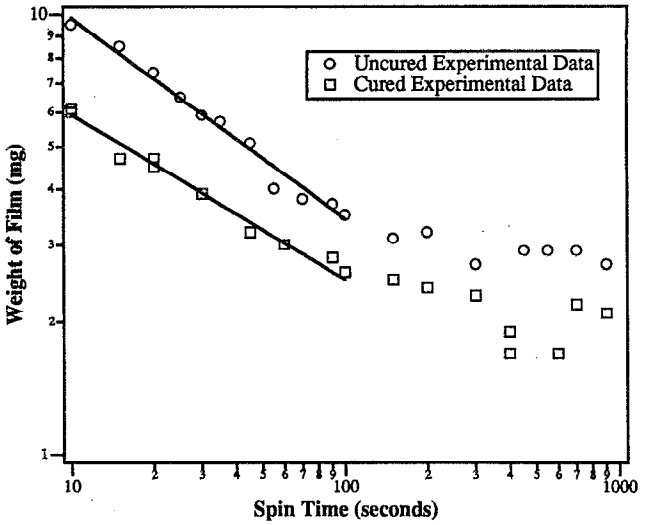

FIG. 11. Dependence of the final film weight on spin time for PI2525 Du Pont polyimide. The rotational speed was 4000 rpm and the films were spun casted onto 25 mm glass cover slides. The cured films included a soft bake at 170 °C followed by ramp and cure step at 400 °C for 30 min. Uncured films were stored under vacuum conditions to remove any remaining solvent until their weight no longer changed. The final film weight appears to depend on spin time for times less than 100 s at these conditions.

relation for the mass transfer coefficient, Eq. (36), shows that the mass transfer coefficient k is proportional to the $\omega^{1/2}$; therefore, H_c must be proportional to $\omega^{-1/2}$. Since $\mathrm{Sh}_c \sim H_c k$, it is independent of the rotational speed, and h_f/H_c must be independent of ω. Therefore, we can always conclude that

$$h_f \sim \omega^{-1/2}. \tag{81}$$

Then how does one explain the -0.8 dependence arrived at by Daughton and Givens? During their experimental investigation, these authors spun their films for 20 s. The curves in Fig. 10 were calculated based on the assumption that spinning continued until the rate of film thinning was dominated by solvent evaporation. For high-viscosity polyimide solutions, the time required for this dominance may be greater than 20 s. In fact the dependence of final film thickness on spin time was determined experimentally for PI2525 at 4000 rpm. Figure 11 shows the final weight of film, assumed to be proportional to the film thickness, as a function of spin time. Included are both cured and uncured films although the uncured films correspond more directly to the model since the shrinkage resulting in imide ring closures during the curing step was not included.

Notice that the final film thickness was found to depend on the spinning time for times shorter than some characteristic quantity, in this case approximately 100 s. This time where film thickness becomes independent of spinning time corresponds to the minimum point in the model where the mass transfer has dominated and the fluid convection is no longer important. Figure 12 is a plot of the final film thickness versus spinning time calculated using the model. The physical parameters were chosen so that they would be as similar to those conditions in Fig. 11 as possible. The model predicts that the final film thickness does depend on the spin time until it reaches a certain value. The discrepancies in the slope and characteristic time are caused by the fact that the value chosen for the mass transfer coefficient is an estimate and is most likely too large.

The experimental results of Daughton and Givens, where the power-law dependence was found to be -0.8, were made for spin times of 20 s. This is most likely too small to be in the region where the final thickness is independent of spin time. All previous models that predicted a power of $-\frac{1}{2}$ implicitly assumed that this condition was

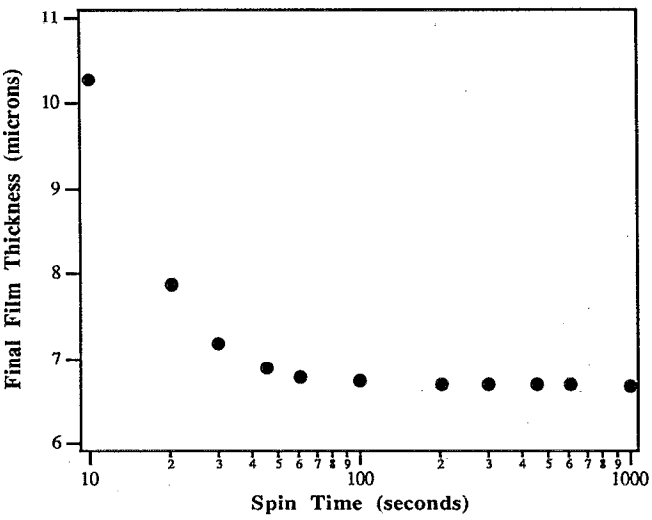

FIG. 12. Model prediction for the dependence of final film thickness on spin time. The physical parameters were based on the experimental values determined for PI2525 and the rotational speed was set to 4000 rpm so that the conditions correspond as closely as possible to Fig. 11.

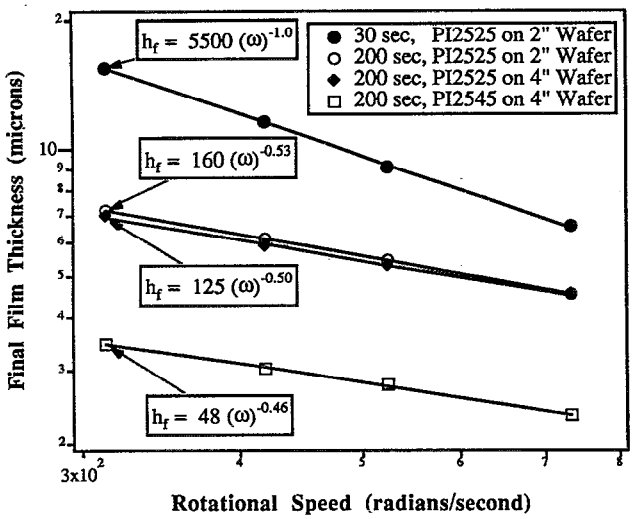

FIG. 13. Model prediction of final film thickness as a function of rotational speed. The 30 s spin time curves represent the situation where spinning is assumed to continue until the mass transfer has dominated and fluid convection is negligible. The 200 s spin time curve represents the case where spinning was discontinued prior to this dominance.

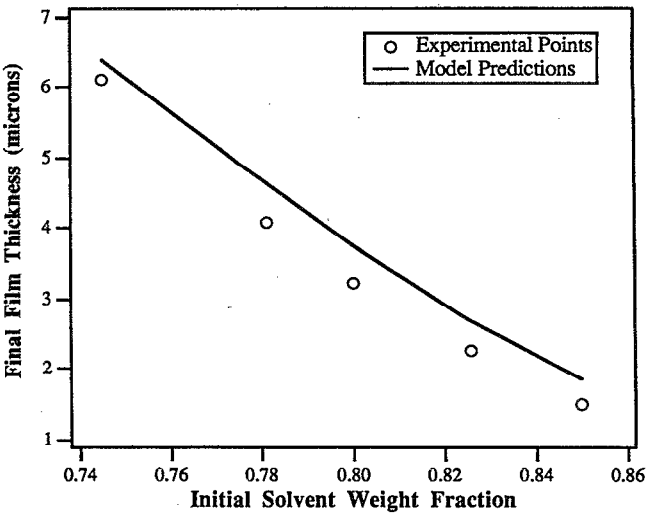

FIG. 14. Dependence of final film thickness on initial weight fraction for Du Pont PI2525 polyimide. Experimental films were spun at 4000 rpm for 500 s and then dried under vacuum. Data points are averages of three samples for the 15% and 20% solutions and two samples for the rest. The physical parameters and spinning conditions for the model were chosen to mimic the experimental conditions.

met. Based on conditions typical for polyimide spin coating and a 30 s total spin time, the model developed here predicts a slope of -0.7 for the power-law dependence of the dry film on rotational speed. Figure 13 shows the effect of spin time on the experimental exponent of this power-law dependence. The data for the 200 s spin on 2 in. wafers is an average of three separate disks where the standard deviation in film thickness ranged from 1% to 2.5% of the average. The remainder of the data is an average of two or three samples with similar reproducibility. Notice that for 30 s spin times using PI2525, the data do not yield the predicted $-\frac{1}{2}$ power dependence. However, when the spin time is long enough that fluid flow is negligible compare to solvent evaporation for the film thinning process (spin times greater than 100 s), the dependence of film thickness on rotational speed will follow the $-\frac{1}{2}$ prediction. This result was found to be true for both polyimide precursor solutions and on 4 in. as well as 2 in. wafers. Therefore, it is essential that the total spinning time of any experimental data is long enough that the final film thickness is independent of spin time before any comparisons to theory are made.

In addition to the rotational speed dependence, the effect of changing the initial solvent weight fraction was investigated. Note that as w_{s0} is changed, both H_c and Sh_c change due to the changing physical parameters. Figure 14 illustrates the effect of changing the initial solvent weight fraction from 0.745 to 0.85. No values outside this range were chosen as solutions more concentrated in polymer than the stock solution value of 0.745, as discussed in Sec. II are extremely difficult to produce. Further, those solutions more dilute than 0.85 were so inviscid that they would not leave a discernible film. The model seems to correlate the experimental data well. The data seem linear over a small range of weight fractions, although this is by no means expected to be true over the entire range.

B. Applicability of the uniform film thickness assumption

Finally, the applicability of the uniform film assumption used for this and previous models was examined. Nonuniform initial film thicknesses have been shown theoretically to reduce naturally to uniform film thicknesses[8,17,46] for zero and low solvent evaporation rates. However, Reisfeld, Bankoff, and Davis[47] predicted an oscillatory deviation of film thickness on the free surface for values of Peclet number between 1 and 100 and for larger values of the mass transfer rate. This later result has been confirmed experimentally by Spangler, Torkelson, and Royal,[48] who found oscillatory thickness values for spin-coated films. However, they professed that these oscillations were damped out when the solvent had a small vapor pressure, when the solvent was considered a good solvent, and when the initial concentration of polymer was above its entanglement point. Each of these situations describes the polyimide precursor-NMP system. Therefore we expect any oscillations to be minimal and of large wavelength.

Table II summarizes the data on 2 and 4 in. wafers. For the 2 in. wafers, only two measurement locations were tested: One was near the center while the other was near the edge. On the 4 in. wafers, four samples were taken spread radially over the wafer. The relative error was calculated for the film thickness measurements on each wafer and was defined to be the average percentage deviation from the mean value. We use this definition rather than using the standard deviation because the number of samples is so small. In each case, the relative error is less than 3%. For the 4 in. wafers, there is a definite trend of the film thickness values decreasing with radial position; however,

TABLE II. Relative errors of film thickness measurements.

Wafer size (in.)	Spin speed (rpm)	(Relative error) × 100%
2	3000	1.03%
2	2000	1.65%
2	4000	<0.01%
2	7000	0.58%
4	3000	1.13%
4	4000	2.70%
4	5000	2.18%
4	7000	2.42%

the slopes are small with an average difference of 0.25 μm between the center and the edge of the wafer. Therefore, the assumption of uniform film thickness is reasonably accurate and any small deviations should not significantly affect the conclusions of this model.

VIII. CONCLUSIONS

A thorough investigation of the mass and momentum equations pertaining to the spin-coating process has been performed. By assuming an uniform film thickness, a one-dimensional model was developed to study the importance of the coupling between fluid flow and mass transfer. A scaling analysis proved the inertial and surface tension forces to be negligible and yielded two characteristic parameters that completely described the spin-coating process. These quantities, which contain the physical parameters, initial solvent content, and spinning conditions, are a characteristic film thickness H_c and a Sherwood number Sh_c defined as follows:

$$H_c=\left(\frac{k\eta_0[\Phi(w_{s0})w_{s0}-w_{s\infty}^g]}{\rho\omega^2}\right)^{1/3},$$

$$\mathrm{Sh}_c=\frac{kH_c[\Phi(w_{s0})w_{s0}-w_{s\infty}^g]}{D_0}.$$

The model predictions were superimposed onto one universal curve with predictive capabilities.

Also, the confusion in the literature over the exponent of the power-law dependence of the final film thickness on the rotational speed was explained. The model predicted an exponent of $-\frac{1}{2}$ which agreed with most experimental investigations. This prediction required that spinning continued long enough that fluid flow has become negligible and solvent evaporation is the dominant mechanism for film thinning. However, when the total spin time was so short that this dominance has not yet occurred, the exponent deviated from $-\frac{1}{2}$. Finally, the split mechanism model, which assumed that the spin-coating process could be divided into two stages, one where fluid flow is occurring exclusively and the other where only mass transfer occurs, was compared to the complete model. The calculations showed that significant quantitative errors developed when using the split approximation.

ACKNOWLEDGMENTS

This work was supported in part by the Office of Naval Research and Amoco Chemical Company. We appreciate the assistance of Ruby Liao, Deane Walker, Lisa Cheung, and Lisa Dorhmann in performing some of the experiments. Also, the profilometer traces were taken by Greg Mulhern in the Berkeley Microfabrication Laboratory.

[1] D. E. Bornside, C. W. Macosko, and L. E. Scriven, J. Imaging Technol. **13**, 122 (1987).
[2] B. T. Chen, Polym. Eng. Sci. **23**, 399 (1983).
[3] G. F. Damon, in *Proceedings of the Second Kodak Seminar on Microminaturization* (Eastman Kodak Co., Rochester, NY, 1967), p. 36.
[4] J. H. Lai, Polym. Eng. Sci. **19**, 1117 (1979).
[5] W. J. Daughton and F. L. Givens, J. Electrochem. Soc. **129**, 173 (1982).
[6] F. L. Givens and W. J. Daughton, J. Electrochem. Soc. **126**, 269 (1979).
[7] P. O'Hagan and W. J. Daughton, Proc. Kodak Seminar Microelectron. **G-48**, 95 (1977).
[8] A. G. Emslie, F. T. Bonner, and L. G. Peck, J. Appl. Phys. **29**, 858 (1958).
[9] P. C. Sukanek, J. Imaging Technol. **11**, 184 (1985).
[10] B. D. Washo, IBM J. Res. Dev. **21**, 190 (1977).
[11] T. Ohara, Y. Matsumoto, and H. Ohashi, Phys. Fluids A **1**, 1949 (1989).
[12] D. Meyerhofer, J. Appl. Phys. **49**, 3993 (1978).
[13] W. W. Flack, D. S. Soong, A. T. Bell, and D. W. Hess, J. Appl. Phys. **56**, 1199 (1984).
[14] D. E. Bornside, C. W. Macosko, and L. E. Scriven, J. Appl Phys. **66**, 5185 (1989).
[15] S. A. Jenekhe, Indian Eng. Chem. Fundam. **23**, 425 (1984).
[16] S. Shimoji, Jpn. J. Appl. Phys. **26**, L905 (1987).
[17] S. A. Jenekhe and S. B. Schuldt, Indian Eng. Chem. Fundam. **23**, 432 (1984).
[18] C. J. Lawrence, Phys. Fluids **31**, 2786 (1988).
[19] T. J. Rehg and B. G. Higgins, Phys. Fluids **31**, 1360 (1988).
[20] L. M. Peurrung and D. B. Graves, J. Electrochem. Soc. **138**, 2115 (1991).
[21] W. Brodkorb, J. M. Köhler, and O. Rizel, Exp. Tech. Phys. **37**, 527 (1989).
[22] L. E. Stillwagon and R. G. Larson, Phys. Fluids A **2**, 1937 (1990).
[23] D. B. La Vergne and D. C. Hofer, Proc. SPIE **539**, 115 (1985).
[24] D. E. Bornside, C. W. Macosko, and L. E. Scriven, J. Electrochem. Soc. **138**, 317 (1991).
[25] C. C. Lin and L. A. Segal, *Mathematics Applied to Deterministic Problems in the Natural Sciences* (Macmillian, New York, 1974).
[26] M. M. Denn, *Process Fluid Mechanics* (Prentice-Hall, Englewood Cliffs, NJ, 1980).
[27] B. G. Higgins, Phys. Fluids **29**, 3522 (1986).
[28] E. M. Sparrow and J. L. Gregg, J. Heat Transfer **82**, 294 (1960).
[29] F. Kreith, J. H. Taylor, and J. P. Chong, J. Heat Transfer **81**, 95 (1959).
[30] J. P. Flory, *Principle of Polymer Chemistry* (Cornell University Press, Ithaca, NY, 1953).
[31] S. A. Jenekhe, Polym. Eng. Sci. **23**, 830 (1983).
[32] S. Middleman, J. Appl. Phys. **62**, 2530 (1987).
[33] R. Keunings, J. Comput. Phys. **62**, 199 (1986).
[34] G. Strang and G. J. Fix, *An Analysis of the Finite Element Method* (Prentice-Hall, Englewood Cliffs, NJ, 1973).
[35] J. N. Reddy, *Applied Functional Analysis and Variational Methods in Engineering* (McGraw-Hill, San Francisco, 1986).
[36] J. N. Reddy, *An Introduction to the Finite Element Method* (McGraw-Hill, NY, 1984).
[37] I. Burdick & Jackson Laboratories, *Solvent Guide* (Burdick & Jackson Laboratories, Inc., Muskegon, MI, 1980).
[38] C. E. Sroog, A. L. Endrey, S. V. Abramo, C. E. Berr, W. M. Edwards, and K. L. Olivier, J. Polym. Sci. Part A **3**, 1373 (1965).
[39] A. Weill, Springer Proc. Phys. **13**, 51 (1986).
[40] *Instrument Manual for D200 Digital Recording Balance* (Cahn, Cerritos, CA, 1990).
[41] A. W. Czanderna and S. P. Wolsky, Eds., *Methods and Phenomena 4:*

Microweighing in Vacuum and Controlled Environments (Elsevier, London, 1980).
[42]M. G. McMaster, masters thesis, University of California, Berkeley, 1988.
[43]R. K. Yonkoski, Ph.D. thesis, University of California, Berkeley, 1992.
[44]R. B. Bird, W. E. Stewart, and E. D. Lightfoot, *Transport Phenomena* (Wiley, New York, 1960).
[45]J. Perry, *Perry's Chemical Engineering Handbook* (McGraw-Hill, San Francisco, 1984).
[46]B. Reisfeld, S. G. Bankoff, and S. H. Davis, J. Appl. Phys. **70**, 5258 (1991).
[47]B. Reisfeld, S. G. Bankoff, and S. H. Davis, J. Appl. Phys. **70**, 5267 (1991).
[48]L. L. Spangler, J. M. Torkelson, and J. S. Royal, Polym. Eng. Sci. **30**, 644 (1990).